Journal of Engineering Science and Technology
Vol. 12, No. 11 (2017) 2922 - 2938

PREDICTION OF LEAKAGE FLOW AND ROTORDYNAMIC CHARACTERISTICS FOR AN ECCENTRIC LABYRINTH GAS SEAL

MOHAMED KAMOUNI

Sidi Mohamed ben Abdellah University, High School of Technology,
Post box 2427, Road of Imouzzer, Fez, Morocco
E-mail: mohamed.kamouni@usmba.ac.ma

Abstract

Labyrinth seals are key elements to limit leakage flow between rotating and stationary parts of turbo machines. However, these seals can modify the rotordynamic stability of machines. Thus, accurate predictions of static and dynamic behaviour for labyrinth seals are very important to optimize efficiency and operating conditions of rotating machines using this kind of seals. The present work contributes by a numerical model based on CFD computation to predict leakage flow and rotordynamic coefficients for a short eccentric labyrinth seal with four teeth fixed on the rotor. The developed model accuracy has been validated on experimental measurements of the pressure distribution along and around the seal which drops from 110770 Pa at the seal inlet to 103300 Pa at the seal outlet. A parametric study has been conducted to show the effect of pressure ratio and inlet swirl ratio on leakage flow and rotordynamic coefficients of the seal. In this study, the outlet pressure is kept constant but the inlet/outlet pressure ratio varies from 1.072 to 8 while three inlet swirl ratios (0, 0.5 and 1) are considered. Obtained results of this work are presented to help designers and industrials optimizing operating conditions and improving performances of this kind of seals.

Keywords: Labyrinth seal, leakage flow, Rotordynamic coefficients, inlet swirl velocity, whirl frequency.

1. Introduction

Labyrinth seals are widely used to reduce leakage in various kinds of turbomachines including turbines, turbo-pumps and compressors. Like bearings in a rotor assembly, these seals have similar rotordynamic force coefficients and

Nomenclatures

C	Sealing mean clearance, m
D	Direct damping cefficient, N.s.m^{-1}
d	Cross-coupled damping cefficient, N·s.m^{-1}
e	Eccentricity, m
F_r	Force component in radial direction, N
F_t	Force component in tangential direction, N
F_y	Force component in y-direction, N
F_z	Force component in z-direction, N
K	Direct stiffness coefficient, N.m^{-1}
k	Cross-coupled stiffness coefficient, N.m^{-1}
P_{in}	Inlet pressure, Pa
P_{out}	Outlet pressure, Pa
PR	Pressure ratio (P_{in}/P_{out})
R	Rotor radius, m
t	Time, s
u_i , u_j	Velocity components in the coordinate system, m.s^{-1}
W_{in}	Inlet preswirl velocity, m.s^{-1}
x_i, x_j	Coordinate system components, m
y, z	Position components of the rotor center, m
$\dot{y}$, $\dot{z}$	Temporal derivation of y and z components, m.s^{-1}

Greek Symbols

δ	Whirling ratio (Ω/ω)
ε	Eccentriciy ratio (e/C)
θ	Anglular position of the rotor center relative to the x axis, deg
λ	Inlet preswirl ratio ($W_{in}/R\omega$)
μ	Dynamic viscosity, kg.m^{-1}s^{-1}
ρ	Density, kg.m^{-3}
Ω	Angular frequency of rotor whirling, rad.s^{-1}
ω	Angular frequency of rotor spin, rad.s^{-1}

generate fluid response forces that can either improve (stabilizing forces) or degrade (destabilizing forces) the dynamic stability of rotor systems [1]. These seal forces, caused by non-uniform circumferential pressure distribution, must be controlled to ensure that the rotor-bearing system remains stable throughout its operational envelope. In order to meet the sealing requirement as defined by the design constraints and required sealing effectiveness, designers have developed many labyrinth seal types: straight, stepped, staggered, inclined, etc. [2]. The complex working flow passing through labyrinth seals has been the subject of many worldwide theoretical and experimental studies in the last three decades. However, various disagreements have been reported between rotordynamic predictions and measurements for these seals. Thus, prediction of leakage and rotordynamic coefficients remains a demanding and challenging task for labyrinth gas seals [3].

In the field of seals' rotordynamic experimental research, Benckert and Wachter [4] were among the first authors to present an early experimental investigation on the rotordynamic characteristics of straight labyrinth seals using

a test rig applying hydraulic shakers to excite the seal stator. They measured the frequency-independent direct and cross-coupled stiffness coefficients for different labyrinth geometries and first discussed the effects of pressure ratio, rotational speed, and inlet flow conditions on the rotordynamic stability of labyrinth seals. Their investigations have proven that the lateral force component acting at a right angle to the rotor deflection plane, represents a vibration exciting force, which has to be accounted for in rotordynamics. They reported that with increasing shaft circumferential speed - pressure ratio constant -, the lateral force is growing. Additionally, for short seals, some swirl webs in front of the first cavity of the seal are sufficient to reduce the preswirl and therefore the lateral force sensitivity.

Childs and Scharrer [5, 6] and Picardo and Childs [7] measured the rotordynamic force coefficients of straight labyrinth seals with teeth on rotor or teeth on stator at various pressure ratios, rotational speeds, sealing clearances and inlet swirl velocities. Their results show that the teeth on stator labyrinth seal is more stable due to lower cross-coupled stiffness values. Also, the effective damping of the labyrinth seal is almost completely insensitive to changes in sealing clearance. Furthermore, it has been showed that labyrinth seals possess frequency-independent rotordynamic coefficients up to a frequency 150 Hz.

Kwanka et al. [8] and Pugachev and Deckner [9] measured the stiffness and damping coefficients of staggered labyrinth seals using a test rig applying magnetic bearing to excite the seal rotor. They presented the effects of pressure ratio, inlet swirl, rotational speed, and rotor eccentricity on the seal stiffness and damping. Their obtained results show that direct stiffness is negative and static direct stiffness increases strongly with the leakage while the dynamic direct stiffness varies only slightly. The measured cross-coupled stiffness decreases with increasing rotational speed while the measured direct stiffness remains relatively constant. They added that damping coefficients are more sensitive to the rotor eccentricity values with a maximum deviation of about 20% at the largest eccentricity. To explain some discrepancies between measurements and predictions for dynamic coefficients, they reported that direct stiffness is particularly sensitive to the measuring method and the inflow cavity used for creating the inlet swirl can generate a significant force at certain operating conditions.

Theoretical rotordynamic modelling of labyrinth seals was mainly based on the bulk-flow approach which continues to be used in the industry [10]. Iwatsubo was the first to develop this approach in 1980 [11]. He presented a one-control-volume bulk-flow model to predict the cavity pressure, circumferential-velocity distribution, and rotordynamic coefficients of a labyrinth seal. He showed that a continuous vortex in the circumferential direction occurs in the fluid flow and its form is like a sinusoidal wave which is rotating in the same direction as the rotor. The primary advantage of bulk-flow models is that they can predict the seal rotordynamic coefficients with efficient computational time. However, these models lack flow details and rely on empirical corrections such as flow coefficients and friction factors [12, 13] that may change for varying operational conditions and seal geometry.

Due to the limitations of this approach, the computational fluid dynamic (CFD) methods are more and more applied everywhere for solving Navier-

Stokes equations to obtain more satisfactory predictions at different boundary and operating conditions. In a general way, with the increased availability of computational resources, comprehensive CFD models are now gradually replacing analytical approaches to predict and simulate thermal and dynamical behaviours in porous mediums as in the works of Adegun et al. [14] where a dynamic analysis has been developed for an incompressible flow through a porous landfill and Pakdee et al. [15] where a premixed combustion has been simulated in a porous media. Moreover, in the same field, Chand el al. [16] have also developed a heat convection parametric study in a nanofluid layer in a porous medium based on Galerkin method.

Currently, several recent works applied commercial CFD codes to labyrinth gas seal rotordynamic problems [17, 18]. In 2012, Pugachev et al. [18] have used a full 3D eccentric CFD model built in ANSYS CFX to predict rotordynamic coefficients of a short staggered three-toot-on-stator labyrinth seal. They reported that the SST turbulence model shows robust performance, however, for highly pre-swirled flows, the turbulence production terms should be limited. Otherwise the SST model over-predicts the cross-coupled stiffness coefficients. Then more recently, in 2016, Sun et al. [19] have studied the effect of swirl brakes on labyrinth seals using a CFD model. Their obtained results show that the swirl brakes play an important role in decreasing the inlet swirl ratio of the seal (60 to 75% less). In addition, by using swirl brakes at the seal entrance, the seal destabilizing forces (cross-coupled stiffness coefficients) decrease (50 to 300% less) while the seal direct damping coefficients increase (50 to 60% larger).

From these numerous applications, one can conclude that CFD technique is a powerful tool, but the accuracy of predictions compared to measurements is not always sufficient and thus, further research is still needed to make CFD calculations a standard of the design process for the prediction of rotordynamic coefficients of labyrinth gas seals. In this context, the present research attempts to calculate the leakage flow and rotordynamic forces through an eccentric short labyrinth gas seal based on three-dimensional CFD techniques solving the general Reynolds Averaged Navier-Stokes equations along with appropriate turbulence model.

2. Geometry and CFD Model of the Seal

2.1. Seal geometry

The straight labyrinth seal object of this study has four teeth fixed on the rotor lateral surface. These teeth generate three cavities in the seal. Figure 1 shows the 2-D seal geometry for a centred position of the rotor with respect to the stator.

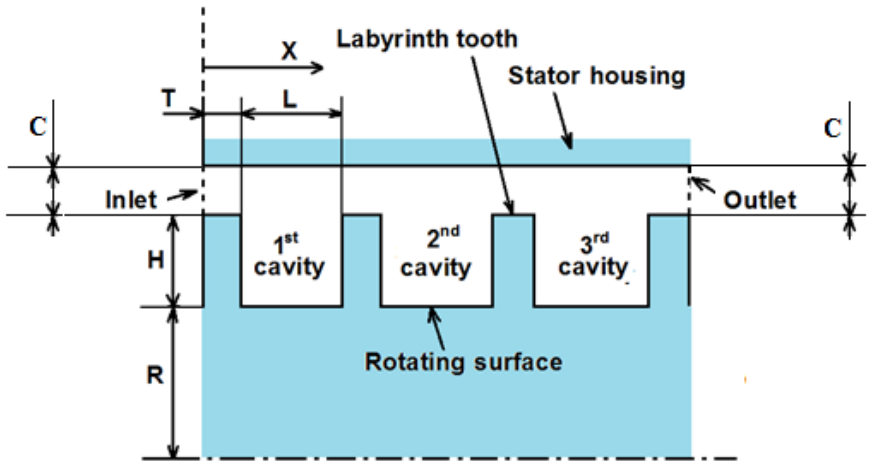

Fig. 1. Labyrinth seal geometry.

The geometrical parameters shown in the 2-D seal geometry are defined and summarized in Table 1.

Table 1. Dimensions of the seal.

Parameter	Value
Rotor radius, *R* (mm)	93.66
Tooth width, *L* (mm)	12.7
Tooth thickness, *T* (mm)	3.18
Tooth height, *H* (mm)	7.94
Mean clearance width, *C* (mm)	0.949

The seal working fluid is air. A cut section of the 3-D fluid computational domain is shown in Fig. 2. The teeth are represented by circumferential grooves in this computational domain.

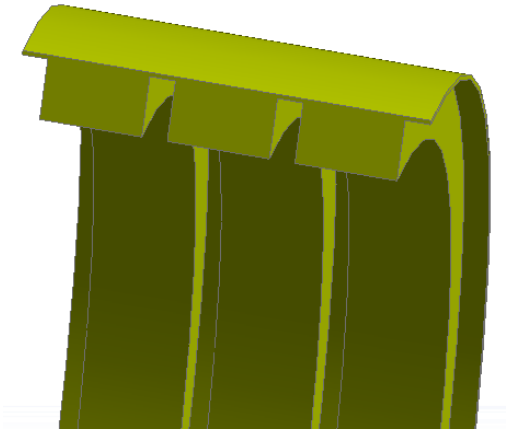

Fig. 2. A cut section of the 3-D computational domain of the seal.

2.2. Governing equations

The turbulent flow through the seal is governed by the continuity and momentum equations.

Continuity equation:

$$\frac{\partial \rho}{\partial \mathrm{t}} + \frac{\partial(\rho U_i)}{\partial x_i} = 0 \tag{1}$$

Momentum equation:

$$\frac{\partial \rho U_i}{\partial t} + \frac{\partial(\rho U_i U_j)}{\partial x_j} = -\frac{\partial p'}{\partial x_i} + \frac{\partial}{\partial x_j}\left[\mu_{eff}\left(\frac{\partial U_i}{\partial x_j} + \frac{\partial U_j}{\partial x_i}\right)\right] + S_M \tag{2}$$

where i and j are the indexes relating to the three directions of space, S_M is the sum of body forces and μ_{eff} is the effective viscosity accounting for turbulence. p' is the modified pressure.

$$p' = p + \frac{2}{3}\rho k + \frac{2}{3}\mu_{eff}\frac{\partial U_k}{\partial x_k} \tag{3}$$

$$\mu_{eff} = \mu + \mu_t \tag{4}$$

where μ_t is the turbulence viscosity and μ is a constant.

The turbulence model assumes that the turbulence viscosity is linked to the turbulence kinetic energy and dissipation via the relation:

$$\mu_t = C_\mu \rho \frac{k^2}{\varepsilon} \tag{5}$$

where C_μ is a constant.

The values of k and ε are obtained directly from the differential transport equations for the turbulence kinetic energy and turbulence dissipation rate:

$$\frac{\partial(\rho k)}{\partial t} + \frac{\partial(\rho U_j k)}{\partial x_j} = \frac{\partial}{\partial x_j}\left[\left(\mu + \frac{\mu_t}{\sigma_k}\right)\frac{\partial k}{\partial x_j}\right] + P_k - \rho\varepsilon + P_{kb} \tag{6}$$

$$\frac{\partial(\rho \varepsilon)}{\partial t} + \frac{\partial(\rho U_j \varepsilon)}{\partial x_j} = \frac{\partial}{\partial x_j}\left[\left(\mu + \frac{\mu_t}{\sigma_\varepsilon}\right)\frac{\partial \varepsilon}{\partial x_j}\right] + \frac{\varepsilon}{k}(C_{\varepsilon 1}P_k - C_{\varepsilon 2}\rho\varepsilon + C_{\varepsilon 1}P_{\varepsilon b}) \tag{7}$$

where $C_{\varepsilon 1}$, $C_{\varepsilon 2}$, σ_k, and σ_ε are constants. P_{kb} and $P_{\varepsilon b}$ represent the influence of the buoyancy forces. P_k is the turbulence production due to viscous forces, which is modelled with:

$$P_k = \mu_t\left(\frac{\partial U_i}{\partial x_j} + \frac{\partial U_j}{\partial x_i}\right)\frac{\partial U_i}{\partial x_j} - \frac{2}{3}\frac{\partial U_k}{\partial x_k}\left(3\mu_t\frac{\partial U_k}{\partial x_k} + \rho k\right) \tag{8}$$

2.3. Boundary conditions

The boundary conditions of the seal are as it follows:

- The rotor surface has a circumferential velocity which is the product of rotor rotational speed and rotor radius. The stator surface is static. Standard wall boundary conditions are used for fluid-solid interaction regions.
- At the seal entrance, the inlet pressure P_{in} is equal to the upstream reservoir total pressure and the inlet circumferential velocity w_{in} is given independently (w_{in}= 0%, 50% or 100% of $R\omega$).
- The flow is adiabatic in the seal.
- At the seal outlet, the exit pressure P_{out} is equal to the downstream reservoir static pressure.

2.4. Meshing

For the given seal geometry, an appropriate mesh is required to describe correctly the flow within the seal. Hexahedral mesh elements were used to create three dimensional non-uniform structured meshes in the entire computational domain. An adequate mesh refinement is allowed to the clearance area and boundary layers to accurately calculate desired physical parameters of the flow within the seal. Figure 3 shows a cut section of generated computational grids in the 3-D computational domain.

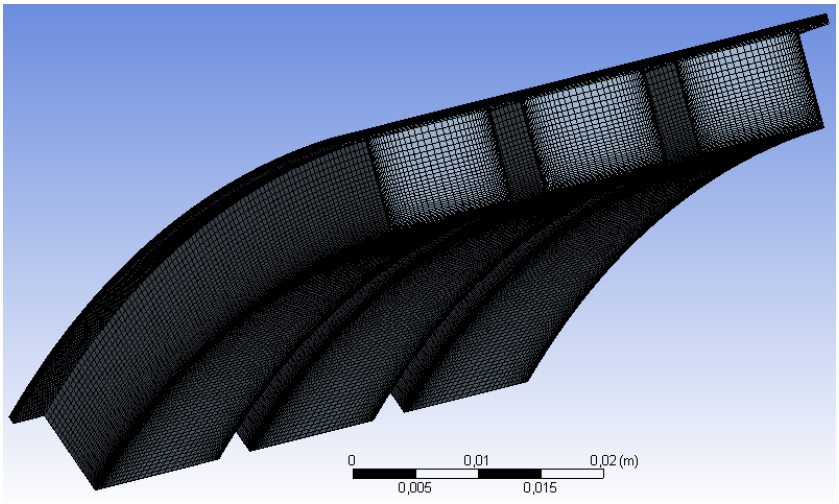

Fig. 3. A cut section of the 3-D Mesh used for the fluid computational domain of the seal.

2.5. Rotating frame

Observing the motion of rotor-seal system from a stationary frame, the rotor is spinning at the speed ω while also whirling at the speed Ω at the same time, which means that the location of rotor and thus the shape of mesh are changing all the time. So, it is actually a transient problem involved with mesh moving. To avoid a transient analysis and moving mesh, a rotating frame with the speed Ω was applied as shown in Fig. 4. In the rotating frame, the rotor itself spins at the

speed (ω-Ω), while the stator spins at the speed Ω in the opposite direction to the frame. Thus, it becomes a steady state problem and there is no mesh moving.

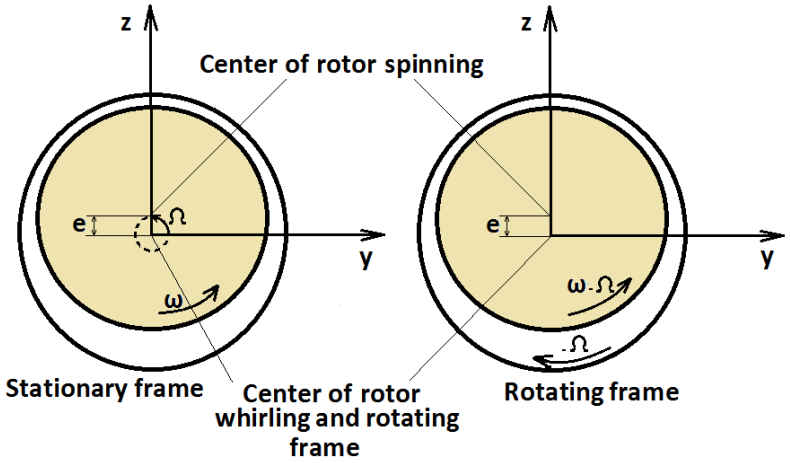

Fig. 4. Frame transfer from stationary to rotating.

2.6. Rotordynamic coefficients

The fluid driving forces acting on the rotor of the seal are represented in Fig. 5. These forces can be obtained at each whirl frequency Ω by integration of the pressure along and around the seal rotor surface.

$$F_y = R\iint p\cos\theta\, d\theta\, dx \tag{9}$$

$$F_z = R\iint p\sin\theta\, d\theta\, dx \tag{10}$$

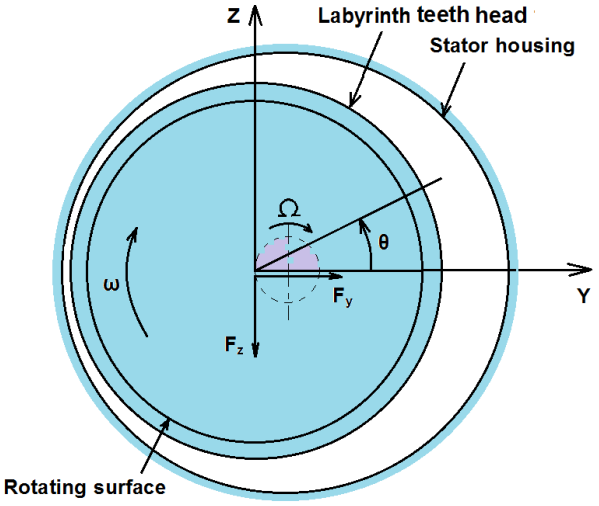

Fig. 5. Fluid forces induced in the seal.

A positive radial force is a centring force while a negative radial force is a decentring one. A positive tangential force is a forward whirl force while a negative tangential force is a backward whirl force. Rotordynamic instability occurs when the forward driving forces exceed the resisting dissipation forces, which leads to self-excitation of the first whirling mode of the rotor [19].

For small motion about a centred position, the relation between the reaction-force components and the shaft motion is defined by the following linearized dynamic model.

$$-\begin{Bmatrix} F_y \\ F_z \end{Bmatrix} = \begin{bmatrix} K & k \\ -k & K \end{bmatrix} \begin{Bmatrix} y \\ z \end{Bmatrix} + \begin{bmatrix} D & d \\ -d & D \end{bmatrix} \begin{Bmatrix} \dot{y} \\ \dot{z} \end{Bmatrix} \tag{11}$$

where (y, z) define the lateral motion of the rotor relative to the stator, (F_y , F_z) are the components of the reaction force acting on the rotor. (K, k) and (D, d) represent the direct and cross-coupled stiffness and damping coefficients, respectively. The cross-coupled terms (k, d) arise from the fluid's circumferential velocity component. If the shaft centre moves in a circular orbit with rayon e, then the rotation displacement vector of the shaft centre has coordinates:

$$y = e.cos\ (\Omega t) \tag{12}$$

$$z = e.sin(\Omega t) \tag{13}$$

The force components acting on the rotor (Fig. 5) can be given from the dynamic equation (11), when $t=0$, as following:

$$\frac{F_r(\Omega)}{e} = \frac{F_y(t=0)}{e} = -d\,\Omega - K \tag{14}$$

$$\frac{F_t(\Omega)}{e} = \frac{F_z(t=0)}{e} = k - D\Omega \tag{15}$$

The direct stiffness coefficient K and the cross coupled damping coefficient d can be obtained employing a linear regression of the calculated radial force for two values of Ω (e.g., Ω = 0 and Ω = 0.5ω) in Eq. (14). The direct damping coefficient D and the cross coupled stiffness coefficient k can be determined from linear regression of the calculated tangential force for two values of Ω (e.g., Ω = 0 and Ω = 0.5ω) in Eq. (15).

3. Results and Discussions

3.1. Validation

To ensure the validity and accuracy of the calculations, the results are compared to available experimental results made on the same seal by Rajakumar and Sisto [20]. The used operating conditions of the seal are summarized in Table 2. The negative signs of the rotating speed and the inlet swirl velocity indicate that the rotor turns in the clockwise direction as per the angle sign convention shown in Fig. 5.

Rajakumar and Sisto [20] have locally measured pressure in each mid-cavity of the seal. Figures 6 and 7 show a comparison of these measurements and the

current CFD predictions for the static pressure distribution along and around the seal, respectively. One can easily see that predictions are in good agreement with experiments. Additionally, Fig. 6 shows that the pressure drops from the inlet pressure at left to the outlet pressure at right, and the pressure is almost equal in each cavity interior.

Table 2. Operating conditions of the seal.

Parameter	Value
Eccentricity ratio, ε	43 %
Rotating speed, ω (rpm)	-2025
Inlet pressure, P_{in} (Pa)	11077 0
Outlet pressure, P_{out} (Pa)	103300
Inlet swirl velocity, W_{in} (ms^{-1})	-49.8

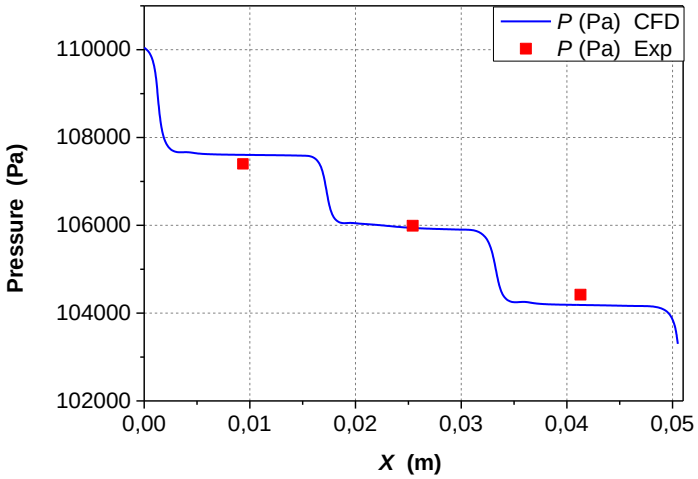

Fig. 6. CFD and experimental pressure distribution in the axial direction of the seal.

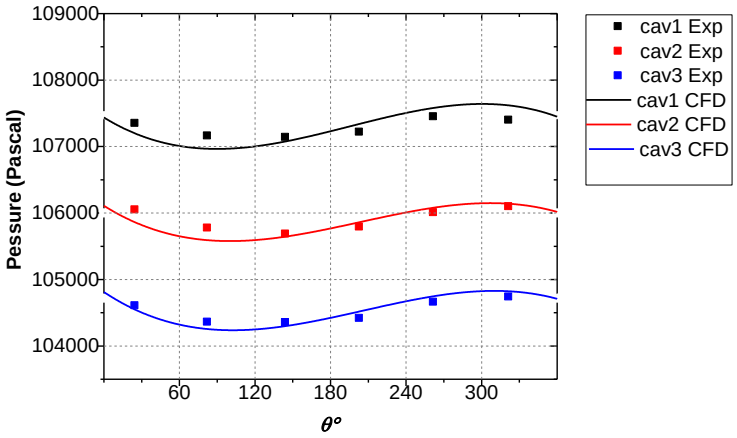

Fig. 7. CFD and experimental pressure distribution in the circumferential direction at the mid-cavities of the seal.

Figure 8 shows contours of the static pressure in the XY plane of the seal. The static pressure drop starts from the seal inlet pressure to reach the outlet pressure at the seal exit. The quasi same colour in each cavity confirms that static pressure is almost constant in each cavity interior. Although no pressure change in the tooth cavity, there is a great pressure drop when the stream flows the tooth gap because the part of the flow is changed into flow speed from static pressure. Furthermore, it is shown that pressure drop mainly occurs in the left zone of each cavity at the labyrinth tooth throttling.

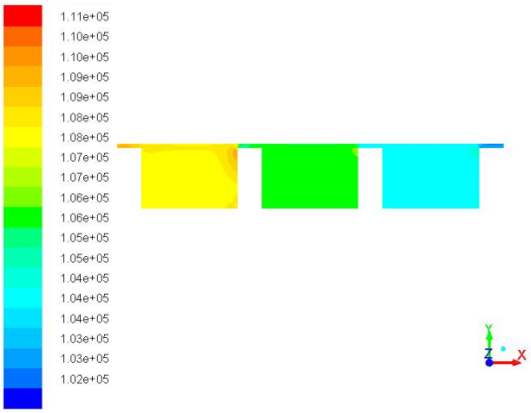

Fig. 8. Pressure contours in the *XY* plane of the seal.

Figure 9 shows the velocity vectors in a radial axial plane of the seal. It can be easily seen that there is a high speed jet at the tip of each tooth and a large vortex inside each chamber. The high pressure drop occurs in the first cavity where a strong flow jet is generated making the flow more turbulent in this cavity. We note that the recirculation zones in the seal cavities act as brakes to stop the axial velocity of the flow through the seal and therefore to reduce the leakage flow. These results confirm the velocity distribution results obtained by Sun et al. [19] in their experimental and numerical studies of labyrinth seals with inlet swirl brakes.

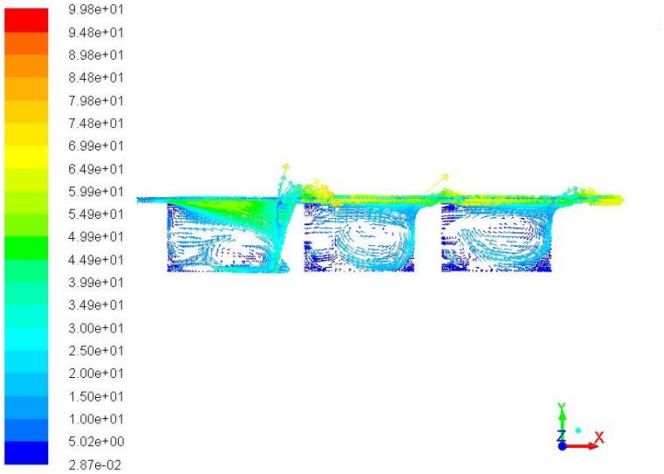

Fig. 9. Velocity vectors in the *XY* plane of the seal.

3.2. Effects of pressure ratio, seal clearance and inlet swirl ratio on leakage flow

Based on the previous operating conditions used to validate the model, we investigated the static behavior of the labyrinth seal through its leakage rate. Figure 10 represents leakage versus the pressure ratio (P_{in}/P_{out}) with the inlet swirl ratio as a parameter. This figure shows that the amount of leakage is more influenced by the inlet/outlet pressure ratio, namely, the leakage increases with increasing pressure ratio. Additionally, it is shown that leakage flow decreases very slightly with increasing inlet swirl to the point that we can consider that the leakage flow through this kind of seals is practically not influenced by the inlet swirl ratio for the envisaged range of pressure ratio.

Figure 11 represents leakage flow versus the pressure ratio (P_{in}/P_{out}) with the mean radial clearance as a parameter. This figure shows that the leakage increases with increasing pressure ratio and mean radial clearance. Furthermore, it can be stated that roughly for this prediction range, the leakage flow increases nearly in the same proportion with increasing mean radial clearance. In addition, the leakage flow becomes more sensitive to pressure ratio variations with high radial clearances. These leakage flow results agree well with the more recent results obtained by Dan Sun et al. [19] and Zhigang et al. [21] for other labyrinth seal configurations and operating conditions.

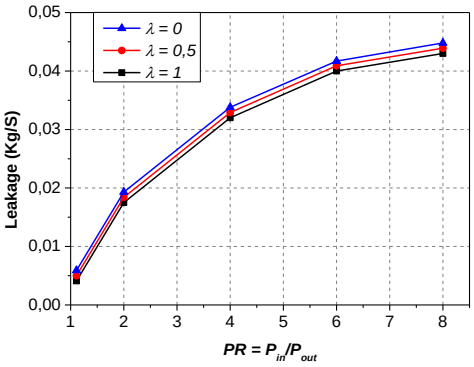

Fig. 10. Leakage flow versus pressure ratio with the inlet swirl ratio as a parameter.

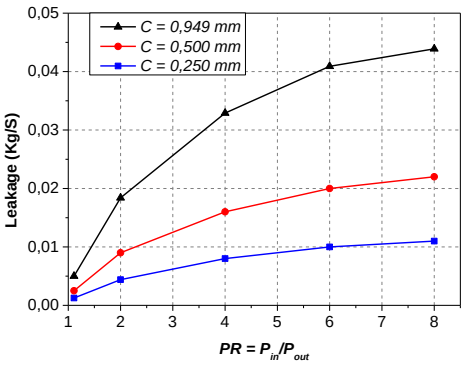

Fig. 11. Leakage flow versus pressure ratio with the mean radial clearance as a parameter.

3.3. Effects of pressure and inlet swirl ratios on dynamic coefficients

The following section deals with the dynamic behaviour of the seal. A parametric study will be conducted with an eccentricity and whirling ratios of 10% and 50% respectively, to analyse the influence of some operating conditions (pressure and inlet swirl ratios) on rotordynamic coefficients of the seal. All other operating conditions remain unchanged.

Figures 12 and 13 represent respectively direct and cross coupled stiffness coefficients versus the pressure ratio (P_{in}/P_{out}) with the inlet swirl ratio as a parameter. It should be noted that the direct stiffness coefficient is always negative and both magnitudes of direct and cross couples stiffness coefficients increase almost linearly with increasing pressure ratio and inlet swirl ratio. These results confirm those obtained by Pugachev et al. [18] in their numerical study relating to CFD prediction of rotordynamic coefficients for short labyrinth seals with other geometry and operating conditions. They also reported that both coefficients of direct and cross-coupled stiffness are linear functions of inlet pressure and the direct stiffness remains negative at all operating conditions. Since the cross coupled stiffness is a destabilizing influence, small values are desired for this coefficient. It results that low pressure and inlet swirl ratios are preferred from a dynamic stability point of view of the seal.

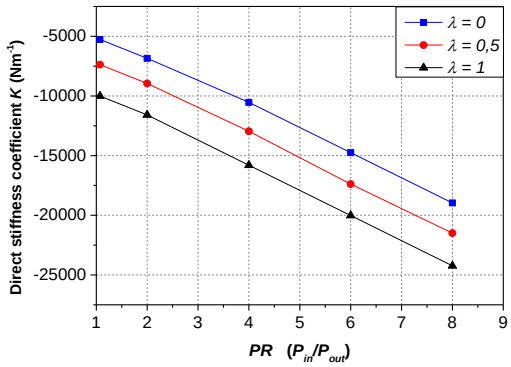

Fig. 12. Direct stiffness coefficient versus pressure ratio with the inlet swirl ratio as a parameter.

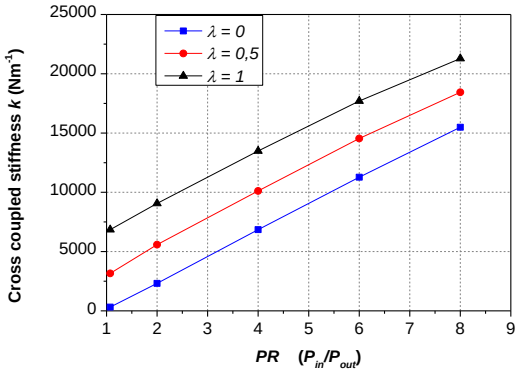

Fig. 13. Cross coupled stiffness coefficient versus pressure ratio with the inlet swirl ratio as a parameter.

Figures 14 and 15 represent respectively direct and cross coupled damping coefficients versus the pressure ratio (P_{in}/P_{out}) with the inlet swirl ratio as a parameter. Both magnitudes of these coefficients increase with increasing pressure and inlet swirl ratios. The direct damping coefficient is a stabilizing influence; hence maximum values are desired for this coefficient. Therefore, high pressure ratio and inlet swirl velocity are beneficial from a dynamic stability point of view of the seal.

Direct damping and cross coupled stiffness coefficients remain the two responsible coefficients for the dynamic stability or instability of the seal. The direct damping is a stabilizing influence while the cross stiffness is a destabilizing influence. The obtained results in Figs. 13 and 14 for these coefficients do not permit to be pronounced about the effect of pressure and inlet swirl ratios on the dynamic stability of the seal. In order to better evaluate this stability, the following whirl frequency ratio will be used.

$$\sigma = \frac{k}{D\Omega} \tag{16}$$

This dimensionless parameter defines, at each whirl frequency Ω, the destabilizing influence of cross coupled stiffness to the stabilizing influence of direct damping. A minimum whirl frequency ratio is preferred from a dynamic stability point of view of the seal.

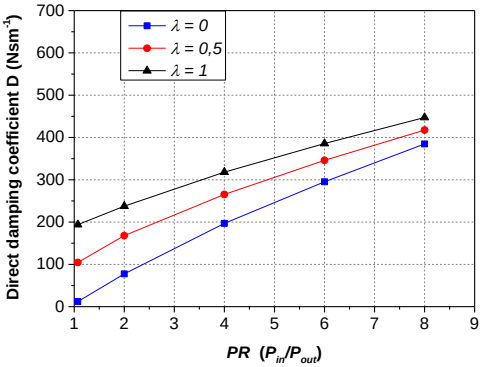

Fig. 14. Direct damping coefficient versus pressure ratio with the inlet swirl ratio as a parameter.

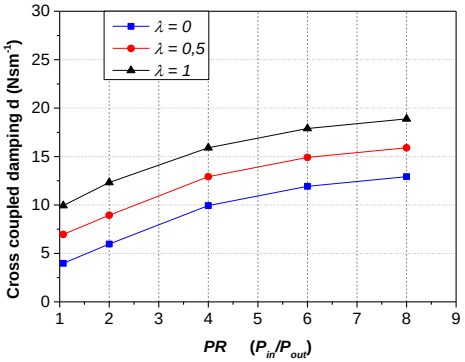

Fig. 15. Cross damping coefficient versus pressure ratio with the inlet swirl ratio as a parameter.

Figure 16 represents the effect of increasing the pressure ratio on the whirl frequency ratio with the inlet swirl ratio as a parameter. This figure shows that whirl frequency ratio increases with increasing pressure and inlet swirl ratios. It can be easily seen that the whirl frequency ratio is minimal for the non-inlet swirl case at low pressure ratios. Otherwise, this figure shows that high positive inlet swirl velocities destabilize more the rotor of this kind of labyrinth seals for the considered range of pressure ratio.

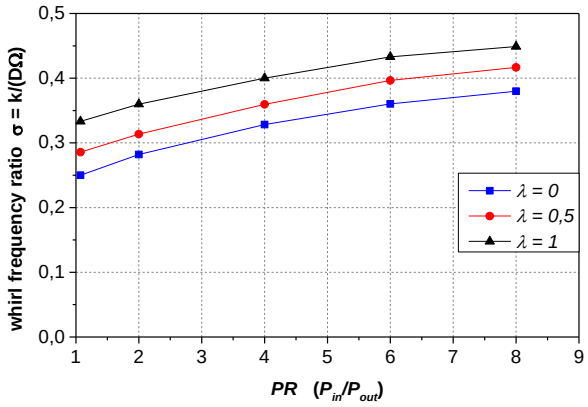

Fig. 16. Whirl frequency ratio versus pressure ratio with the inlet swirl ratio as a parameter.

4. Conclusions

A model to analyse turbulent flow through short eccentric labyrinth seal has been developed based on CFD computation. The model uses the general Reynolds Averaged Navier-Stokes (RANS) equations along with appropriate turbulence model. Some concluding observations from this investigation are given below.

- Predictions of the pressure distribution along and around the seal are in good agreement with measurements on the same seal.
- The pressure is almost quasi equal in each cavity interior and pressure drop mainly occurs in the left zone of each cavity at the labyrinth tooth throttling.
- There is a high speed jet at the tip of each tooth and a large vortex inside each chamber.
- The recirculation zones in the seal cavities act as brakes to stop the axial velocity of the flow through the seal and therefore to reduce the leakage flow.
- The leakage flow through the seal increases with increasing pressure ratio but it decreases very slightly with the inlet swirl ratio increasing for the envisaged range of pressure ratio.
- The leakage flow through the seal increases with increasing pressure ratio and mean radial clearance.
- The leakage flow becomes more sensitive to pressure ratio variations with high radial clearances.

- The direct stiffness coefficient is negative for the envisaged operating conditions of this kind of seals. The magnitude of this coefficient increases almost linearly with increasing pressure ratio and inlet swirl ratio.
- The cross-coupled stiffness coefficient (destabilizing influence) and the direct damping coefficient (stabilizing influence) increase with increasing pressure ratio and inlet swirl ratio.
- The whirl frequency ratio, as a dynamic stability indicator, increases with increasing inlet pressure and inlet swirl velocity. The studied seal remains more stable for the non-inlet swirl case.
- High positive inlet swirl ratios destabilize more this kind of seals for the envisaged operating conditions.

References

1. Vance, J.M. (2010). *Machinery vibration and rotordynamics*. Wiley, New York, USA, 271-278.
2. Chupp, R.E.; Hendricks, R.C.; Lattime, S.B.; and Steinetz, B.M. (2006). Sealing in turbomachinery. *Journal of Propulsion and Power*, 22(2), 313-349.
3. Wensheng, M.; Zhaobo, C.; and Yinghou, J. (2011). Leakage and whirl speed study in labyrinth seal using CFD. *International Conference on Electronic & Mechanical Engineering and Information Technology*, Harbin, China, 592-595.
4. Benckert, H.; and Wachter, J. (1980). Flow induced spring constants of labyrinth seals. *Proceedings of the Second International Conference on Vibrations in Rotating Machinery*, Inst. of Mechanical Engineers, Cambridge, England, U.K, 53-63.
5. Childs, D.; and Scharrer, J. (1986). Experimental rotordynamic coefficient results for teeth-on-rotor and teeth-on-stator labyrinth gas seals. *Journal of Engineering for Gas Turbines and Power*, 108(4), 599-604.
6. Childs, D.; and Scharrer, J. (1988). Theory versus experiment for the rotordynamic coefficient of labyrinth gas seals: part 2 - a comparison to experiment. *Journal of Vibration and Acoustics*, 110(3), 281-287.
7. Picardo, A.; and Childs, D.W. (2005). Rotordynamic coefficients for a tooth on- stator labyrinth seal at 70 bar supply pressures: measurements versus theory and comparisons to a hole-pattern stator seal. *Journal of Engineering for Gas Turbines and Power*, 127(4), 843-855.
8. Kwanka, K.; Sobotzik, J.; and Nordman, R. (2000). Dynamic coefficients of labyrinth gas seals - a comparison of experimental results and numerical calculations. *AMSE International Gas Turbine and Aeroengine Congress & Exhibition, No 2000-GT-0403*, Munich, Germany.
9. Pugachev, A.O.; and Deckner, M. (2010). Analysis of the experimental and CFD - based theoretical methods for studying rotordynamic characteristics of labyrinth gas seals, *Proceedings of ASME Turbo Expo: Power for Land, Sea and Air*. *No GT2010-22058*, Glasgow, UK.

10. Arghir, M.; and Frêne, J. (2004). A bulk-flow analysis of static and dynamic characteristics of eccentric circumferentially-grooved liquid annular seals. *ASME Journal of Tribology*, 126(2), 316-325.
11. Iwatsubo, T. (1980). Evaluation of instability forces of labyrinth seals in turbines or compressors. *Proceedings of Rotordynamic Instability Problems in High Performance Turbomachinery*, *NASA CP-2133*, Texas A&M University, 139-167.
12. Hirs, G.G. (1973). A bulk flow theory for turbulence in lubricant films. *Trans. ASME, Journal of Lubrication Technology*, 95(2), 137-146.
13. Moody, L. (1944). Friction factors for pipe flow. *Transactions of the ASME*, 66, 671-684.
14. Adegun, I.; Komolafe, O.; Hussein, A.K.; and Oyekale, J. (2014). A 3D finite element analysis of incompressible fluid flow and contaminant transport through a porous landfill. *Journal of Engineering Science and Technology* (*JESTEC*), 9(4), 477- 489.
15. Pakdee, W.; Utaivorawit, N.; and Hussein, A.K. (2015). Mathematical model in the form of vorticity-stream function for porous premixed combustion. *Songklanakarin Journal of Science and Technology*, 37(5), 595-600.
16. Chand, R.; Rana, G.; and Hussein, A.K. (2015). On the onset of thermal instability in a low Prandtl number nanofluid layer in a porous medium. *Journal of Applied Fluid Mechanics*, 8(2), 265-272.
17. Moore, J.; Ransom. D.; and Viana, F. (2011). Rotordynamic force prediction of centrifugal compressor impellers using computational fluid dynamics. *ASME, Journal of Engineering for Gas Turbines and Power*, 133(4), 1-10.
18. Pugachev, A.; Kleinhansand, U.; and Gaszner, M. (2012). Prediction of rotordynamic coefficients for short labyrinth gas seals using computational fluid dynamics. *ASME, Journal of Engineering for Gas Turbines and Power*, 134(6), 1-10.
19. Sun, D.S.; Wang, D.; Fei, C.; Ai, Y.; and Wang, K. (2016). Numerical and experimental investigation on the effect of swirl brakes on the labyrinth seals. *ASME, Journal of Engineering for Gas Turbines and Power*, 138(3), 1-12.
20. Rajakumar, C.; and Sisto, F. (1990). Experimental investigations of rotor whirl excitation forces induced by labyrinth seal flow. *ASME, Journal of Vibration and Acoustics*, 112, 515-522.
21. Zhigang, L.; Jun, L.; and Zhenping, F. (2016), Labyrinth seal rotordynamic characteristics part II: geometrical parameter effects. *Journal of Propulsion and Power*, 32(5), 1281-1291.